A Contrivance for a Dynamic Porous Framework: Cooperative Guest Adsorption Based on Square Grids Connected by Amide−Amide Hydrogen Bonds

Kazuhiro Uemura,[†] Susumu Kitagawa,[*,†] Kôichi Fukui,[‡] and Kazuya Saito[§]

*Contribution from the Department of Synthetic Chemistry and Biological Chemistry,
Graduate School of Engineering, Kyoto University, Katsura,
Nishikyo-ku, Kyoto 615-8510, Japan, Regional Joint Research Project of Yamagata Prefecture,
Matsuei 2-2-1, Yamagata 990-2473, Japan, and Research Center for Molecular
Thermodynamics, Graduate School of Science, Osaka University,
Toyonaka, Osaka 560-0043, Japan*

Received December 3, 2003; E-mail: kitagawa@sbchem.kyoto-u.ac.jp

Abstract: Flexible porous coordination polymers containing amide groups as a function origin have been synthesized and categorized as "Coordination Polymer with Amide Groups". Bispyridyl ligands with a spacer of amide group afford two-dimensional (2-D) motifs with a deformed square grid, resulting in three-dimensional (3-D) frameworks of $[Co(NO_3)_2(3\text{-pna})_2]_n$ (**1**), $[Co(Br)_2(3\text{-pna})_2]_n$ (**2**), and $\{[Co(NCS)_2(4\text{-peia})_2]\cdot 4Me_2CO\}_n$ (**3** ⊃ **4Me₂CO**) (3-pna = *N*-3-pyridylnicotinamide, 4-peia = *N*-(2-pyridin-4-yl-ethyl)-isonicotinamide), where the 2-D motifs are bound by complementary hydrogen bond between the amide groups. In the case of the **3** ⊃ **4Me₂CO**, the amide groups form a contrivance for a dynamic porous framework because of their relevant position and orientation in the mutual nearest neighboring motifs. Consequently, **3** ⊃ **4Me₂CO** shows *amorphous* (nonporous)-*to-crystal* (porous) structural rearrangement in the Me₂CO adsorption and desorption process, where the framework of the 2-D motif is maintained. The adsorption isotherm has threshold pressure (P_{th}), a sort of gate pressure. The heat of Me₂CO adsorption ($\Delta H_{ad} = -25$ kJ/mol) is obtained from the temperature dependence of threshold pressure (P_{th}), which is close to acetone vaporization enthalpy ($\Delta H_{vap} = 30.99$ kJ/mol).

Introduction

In a decade, coordination polymers have been extensively studied and added a new dimension to materials-directed coordination chemistry. The synthetic method is rapidly being developed from accidental to rational stage,[1−10] affording porous frameworks, which could be relevant for storage and exchange of specific guests, catalysis, and guest alignment.[11−15] Two

recent targets for the porous coordination polymers is a robust framework such as inorganic zeolites[10,16] and large pores with high specific surface area.[17] In addition to such targets, an approach to create other properties, characteristic of porous coordination polymers, has been explored, and the most interesting is a dynamic micropore, which responds to a chemical stimulus.[18,19] This property could come from a sort of "soft" framework with bistability, whose two states go back from and forth to one of counterparts; a system could exist in one or two states for the same values of external field parameters. Recently, several articles[19−37] have reported dynamic

[†] Kyoto University.
[‡] Regional Joint Research Project of Yamagata Prefecture.
[§] Osaka University.

(1) Batten, S. R.; Robson, R. *Angew. Chem., Int. Ed.* **1998**, *37*, 1460−1494.
(2) Li, H.; Eddaoudi, M.; O'Keeffe, M.; Yaghi, O. M. *Nature* **1999**, *402*, 276−279.
(3) Hagrman, P. J.; Hagrman, D.; Zubieta, J. *Angew. Chem., Int. Ed.* **1999**, *38*, 2638−2684.
(4) Noro, S.-I.; Kitagawa, S.; Kondo, M.; Seki, K. *Angew. Chem., Int. Ed.* **2000**, *39*, 2082−2084.
(5) Seki, K. *Chem. Commun.* **2001**, 1496−1497.
(6) Desiraju, G. R. *Nature* **2001**, *412*, 397−400.
(7) Moulton, B.; Zaworotko, M. J. *Chem. Rev.* **2001**, *101*, 1629−1658.
(8) Zaworotko, M. J. *Chem. Commun.* **2001**, 1−9.
(9) Eddaoudi, M.; Kim, J.; Rosi, N.; Vodak, D.; Wachter, J.; O'Keeffe, M.; Yaghi, O. M. *Science* **2002**, *295*, 469−472.
(10) Yaghi, O. M.; O'Keeffe, M.; Ockwig, N. W.; Chae, H. K.; Eddaoudi, M.; Kim, J. *Nature* **2003**, *423*, 705−714.
(11) Hoskins, B. F.; Robson, R. *J. Am. Chem. Soc.* **1990**, *112*, 1546−1554.
(12) Fujita, M.; Kwon, J. Y.; Washizu, S.; Ogura, K. *J. Am. Chem. Soc.* **1994**, *116*, 1151−1152.
(13) Yaghi, O. M.; Li, H. *J. Am. Chem. Soc.* **1996**, *118*, 295−296.
(14) Kondo, M.; Yoshitomi, T.; Seki, K.; Matsuzaka, H.; Kitagawa, S. *Angew. Chem., Int. Ed. Engl.* **1997**, *36*, 1725−1727.
(15) Langley, P. J.; Hulliger, J. *Chem. Soc. Rev.* **1999**, *28*, 279−291.

(16) Eddaoudi, M.; Moler, D. B.; Li, H.; Chen, B.; Reineke, T. M.; O'Keeffe, M.; Yaghi, O. M. *Acc. Chem. Res.* **2001**, *34*, 319−330.
(17) Noro, S.-i.; Kitagawa, S.; Yamashita, M.; Wada, T. *Chem. Commun.* **2002**, 222−223.
(18) Kitagawa, S.; Kondo, M. *Bull. Chem. Soc. Jpn.* **1998**, *71*, 1739−1753.
(19) Uemura, K.; Kitagawa, S.; Kondo, M.; Fukui, K.; Kitaura, R.; Chang, H.-C.; Mizutani, T. *Chem.−Eur. J.* **2002**, *8*, 3586−3600.
(20) Kitaura, R.; Fujimoto, K.; Noro, S.-i.; Kondo, M.; Kitagawa, S. *Angew. Chem., Int. Ed.* **2002**, *41*, 133−135.
(21) Kitaura, R.; Seki, K.; Akiyama, G.; Kitagawa, S. *Angew. Chem., Int. Ed.* **2003**, *42*, 428−431.
(22) Halder, G. J.; Kepert, C. J.; Moubaraki, B.; Murray, K. S.; Cashion, J. D. *Science* **2002**, *298*, 1762−1765.
(23) Cussen, E. J.; Claridge, J. B.; Rosseinsky, M. J.; Kepert, C. J. *J. Am. Chem. Soc.* **2002**, *124*, 9574−9581.
(24) Biradha, K.; Hongo, Y.; Fujita, M. *Angew. Chem., Int. Ed.* **2002**, *41*, 3395−3398.
(25) Biradha, K.; Fujita, M. *Angew. Chem., Int. Ed.* **2002**, *41*, 3392−3395.
(26) Suh, M. P.; Ko, J. W.; Choi, H. J. *J. Am. Chem. Soc.* **2002**, *124*, 10976−10977.
(27) Seki, K. *Phys. Chem. Chem. Phys.* **2002**, *4*, 1968−1971.

Scheme 1
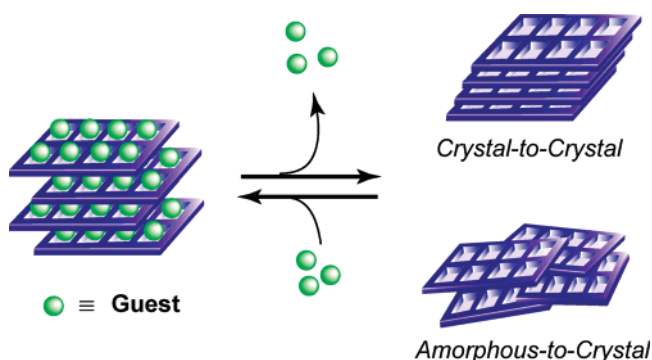
porous coordination polymers which show framework transformation accompanying the adsorption and desorption of guest molecules as shown in eq 1:

$$H + n \cdot G \rightleftarrows H \cdot G_n \ (H \supset n \cdot G) \tag{1}$$

where H is the apohost, G is the guest molecule, and n is stoichiometry of accommodated guest vs apohost.[38] These new types of porous coordination polymers are expected to provide characteristic functionality such as highly selective guest inclusions[19,30] and reversible magnetic modulation.[22,37,39,40]

There are two kinds of forms for apohost; one is "crystal" and the other is "amorphous" (Scheme 1). When an apohost is amorphous, such structural transformation is regarded as "recoverable collapse". Therefore, the approach to create such a transformation could be applicable to brittle materials systems.[41] A unique adsorption property is expected for this amorphous-to-crystal phase transformation. Several coordination polymers recover their crystallinity with the aid of *liquid* solvents, such as in a recrystallization process.[33−35] On the other hand, the transformation to a crystal form merely upon exposure to guest *vapor* has been observed for several compounds.[36,37] A clue for this flexible but ordered structure is to set a contrivance for a framework by which amorphous-to-crystal transformation could be realized. For this purpose, it is useful to take advantage of organic ligands, which possess weak interaction such as a hydrogen bond, and therefore the utilization

could have great contribution to a wide range of framework formation.

Although there are various combinations of hydrogen bond-type gadgets in structural motifs, a layer-type motif would operate well for creating dynamic but reversible porous framework, which exhibits structural transformation caused by external stimuli, the event occurring either within the layer or between the layers.[19,24] When py-X-py (py = pyridine, spacer X = functional group)-type ligands are employed, two-dimensional (2-D) networks are readily formed; straight-type rod ligands have thus far afforded a square grid,[12,24,42−56] rectangular grid,[57−61] herringbone, brick wall, bilayer, and so on.[7,8] Among all the possible networks from py-X-py, the square grid or rectangular grid polymers are of particular importance because they could control the spatial dimensions of grids and chemistry of the interior of channels by modifying the spacer group (X) in the ligand. Once the size of channels in such a square grid system is fixed, another important factor is the stacking modes of the grids in the nearest-neighbor layers. It has been reported that for coordination polymers of planar square grids, three types of stacking modes are typically observed, as follows (Scheme 2):

(i) Edge-to-edge type: grids in the nearest-neighbor layers eclipse in edge-to-edge fashion (or short-slipped manner), designated as ...AAA...[19,24,46,51]
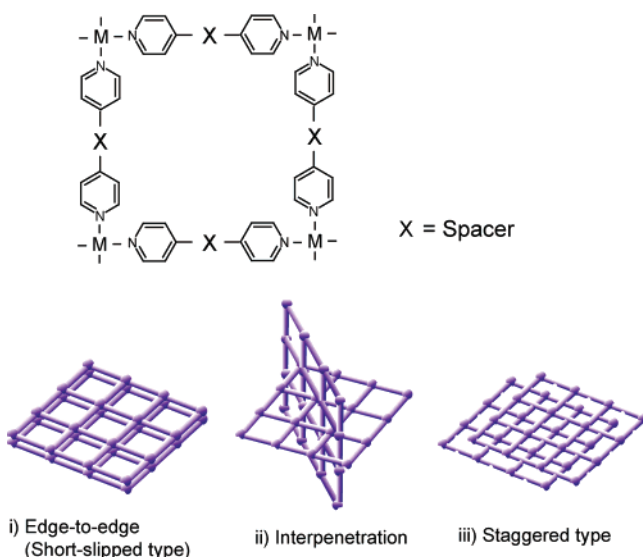
(ii) Interpenetration type: square grids are intimately interlocked with other(s) in the same sort of topological relationship.[42,49,54,56,62,63]

(iii) Staggered type: grids deposit on each other in an offset fashion, designated as ...ABAB... (or ...ABCABC...).[12,43−48,50−53,55]

(28) Takamizawa, S.; Nakata, E.-i.; Yokoyama, H.; Mochizuki, K.; Mori, W. *Angew. Chem., Int. Ed.* **2003**, *42*, 4331−4334.
(29) Serre, C.; Millange, F.; Thouvenot, C.; Nogues, M.; Marsolier, G.; Louer, D.; Ferey, G. *J. Am. Chem. Soc.* **2002**, *124*, 13519−13526.
(30) Makinen, S. K.; Melcer, N. J.; Parvez, M.; Shimizu, G. K. H. *Chem.−Eur. J.* **2001**, *7*, 5176−5182.
(31) Edgar, M.; Mitchell, R.; Slawin, A. M. Z.; Lightfoot, P.; Wright, P. A. *Chem.−Eur. J.* **2001**, *7*, 5168−5175.
(32) Alberti, G.; Brunet, E.; Dionigi, C.; Juanes, O.; Mata, M. J. d. l.; Rodriguez-Ubis, J. C.; Vivani, R. *Angew. Chem., Int. Ed.* **1999**, *38*, 3351−3353.
(33) Choi, H. J.; Lee, T. S.; Suh, M. P. *Angew. Chem., Int. Ed.* **1999**, *38*, 1405−1408.
(34) Min, K. S.; Suh, M. P. *Chem.−Eur. J.* **2001**, *7*, 303−313.
(35) Cao, R.; Sun, D.; Liang, Y.; Hong, M.; Tatsumi, K.; Shi, Q. *Inorg. Chem.* **2002**, *41*, 2087−2094.
(36) Tabares, L. C.; Navarro, J. A. R.; Salas, J. M. *J. Am. Chem. Soc.* **2001**, *123*, 383−387.
(37) Maspoch, D.; Ruiz-Molina, D.; Wurst, K.; Domingo, N.; Cavallini, M.; Biscarini, F.; Tejada, J.; Rovira, C.; Veciana, A. J. *Nat. Mater.* **2003**, *2*, 190−195.
(38) Hereafter, the number n is defined for the ratio of [the amount of adsorbed guest molecules]/[asymmetric unit of the crystal].
(39) Larionova, J.; Chavan, S. A.; Yakhmi, J. V.; Froystein, A. G.; Sletten, J.; Sourisseau, C.; Kahn, O. *Inorg. Chem.* **1997**, *36*, 6374−6381.
(40) Usuki, N.; Ohba, M.; Okawa, H. *Bull. Chem. Soc. Jpn.* **2002**, *75*, 1693−1698.
(41) White, S. R.; Sottos, N. R.; Geubelle, P. H.; Moore, J. S.; Kessler, M. R.; Sriram, S. R.; Brown, E. N.; Viswanathan, S. *Nature* **2001**, *409*, 794−797.

(42) Gable, R. W.; Hoskins, B. F.; Robson, R. *J. Chem. Soc., Chem. Commun.* **1990**, 1677−1678.
(43) Biradha, K.; Hongo, Y.; Fujita, M. *Angew. Chem., Int. Ed.* **2000**, *39*, 3843−3845.
(44) Pschirer, N. G.; Ciurtin, D. M.; Smith, M. D.; Bunz, U. H. F.; Loye, H.-C. z. *Angew. Chem., Int. Ed.* **2002**, *41*, 583−585.
(45) Aoyagi, M.; Biradha, K.; Fujita, M. *Bull. Chem. Soc. Jpn.* **2002**, *73*, 1369−1373.
(46) Biradha, K.; Fujita, M. *J. Chem. Soc., Dalton Trans.* **2000**, 3805−3810.
(47) Bourne, S. A.; Kilkenny, M.; Nassimbeni, L. R. *J. Chem. Soc., Dalton Trans.* **2001**, 1176−1179.
(48) Lu, J.; Paliwala, T.; Lim, S. C.; Yu, C.; Niu, T.; Jacobson, A. J. *Inorg. Chem.* **1997**, *36*, 923−929.
(49) Kondo, M.; Shimamura, M.; Noro, S.-i.; Minakoshi, S.; Asami, A.; Seki, K.; Kitagawa, S. *Chem. Mater.* **2000**, *12*, 1288−1299.
(50) Haynes, J. S.; Rettig, S. J.; Sams, J. R.; Thompson, R. C.; Trotter, J. *Can. J. Chem.* **1987**, *65*, 420−426.
(51) Tong, M.-L.; Ye, B.-H.; Cai, J.-W.; Chen, X.-M.; Ng, S. W. *Inorg. Chem.* **1998**, *37*, 2645−2650.
(52) Biradha, K.; Domasevitch, K. V.; Moulton, B.; Seward, C.; Zaworotko, M. J. *Chem. Commun.* **1999**, 1327−1328.
(53) Biradha, K.; Domasevitch, K. V.; Hogg, C.; Moulton, B.; Power, K. N.; Zaworotko, M. J. *Cryst. Eng.* **1999**, *2*, 37−45.
(54) Real, J. A.; Andres, E.; Munoz, M. C.; Julve, M.; Granier, T.; Bousseksou, A.; Varret, F. *Science* **1995**, *268*, 265−267.
(55) Real, J. A.; Munno, G. D.; Munoz, M. C.; Julvel, M. *Inorg. Chem.* **1991**, *30*, 2701−2704.
(56) Park, S. H.; Kim, K. M.; Lee, S.; Jung, O.-S. *Bull. Korean Chem. Soc.* **1998**, *19*, 79−82.
(57) MacGillivray, L. R.; Groeneman, R. H.; Atwood, J. L. *J. Am. Chem. Soc.* **1998**, *120*, 2676−2677.
(58) Groeneman, R. H.; MacGillivray, L. R.; Atwood, J. L. *Chem. Commun.* **1998**, 2735−2736.
(59) Tong, M.-L.; Chen, X.-M.; Yu, X.-L.; Mak, T. C. W. *J. Chem. Soc., Dalton Trans.* **1998**, 5−6.
(60) Kawata, S.; Kitagawa, S.; Kondo, M.; Furuchi, I.; Munakata, M. *Angew. Chem., Int. Ed. Engl.* **1994**, *33*, 1759−1761.
(61) Zheng, L.-M.; Fang, X.; Lii, K.-H.; Song, H.-H.; Xin, X.-Q.; Fun, H.-K.; Chinnakali, K.; Razak, I. A. *J. Chem. Soc., Dalton Trans.* **1999**, 2311−2316.
(62) Shin, D. M.; Lee, I. S.; Chung, Y. K.; Lah, M. S. *Inorg. Chem.* **2003**, *42*, 5459−5461.
(63) Shin, D. M.; Lee, I. S.; Chung, Y. K.; Lah, M. S. *Chem. Commun.* **2003**, 1036−1037.

Scheme 2

i) Edge-to-edge
(Short-slipped type)

ii) Interpenetration

iii) Staggered type

Scheme 3

3-pia, 3-pna

4-peia

Types ii and iii hinder effective pores, since the cavities in a layer are usually obstructed by adjacent layers. However, even if the interpenetration or staggered manner occurs, we expect the presence of voids for an inclusion of small-molecule when we use longer ligands.[43,49] Square grids of $\{[Ni(L)_2(NO_3)_2]\cdot 4(o\text{-xylene})\}_n$ (L = py-PhPh-py, py = pyridine) in a staggered manner afford large pores,[43] resulting in a three-dimensional (3-D) held porous network.

On this background, we focus on stacking modes of square grids controlled by hydrogen bonds, which are associated with dynamic pores. "Coordination Polymer with Amide Groups" is one of the candidates relevant to those having square grids with hydrogen bonds in staggered fashion, where coordination polymers including L−amide−L-type ligand (L = ligand-containing coordination donor atom) form complementary hydrogen bonding (so-called hydrogen-bond pillar framework) between 2-D motifs. Such a form of hydrogen bond is similar to that of amide binding of cyclic peptide[64,65] and useful for achieving pores in coordination polymers. In this article, new "Coordination Polymer with Amide Groups" (**1**−**3**) based on hydrogen-bond pillar framework were synthesized (Scheme 3), characterized by X-ray crystallography and sorption measurements, and particularly discussed about the adsorption and structural transformation of **3** ⊃ **4Me₂CO** based on thermodynamic analysis.

Experimental Section

Materials. Isonicotinic chloride hydrochloride, nicotinic chloride hydrochloride, 3-aminopyridine, and 4-(2-aminoethyl)pyridine were obtained from Tokyo Kasei Industrial. Co(SCN)₂ was obtained from Aldrich Co.

Synthesis of N-(3-Pyridyl)nicotinamide (3-pna). The ligand was prepared by the reaction of nicotinic chloride hydrochloride (15.2 g, 85 mmol) with 3-aminopyridine (8.0 g, 85 mmol) in dry tetrahydrofuran (220 mL) in the presence of triethylamine (25 mL, 179 mmol) under N₂. The product was recrystallized from acetone/hexane in 47% yield (8.0 g). ¹H NMR (DMSO): δ 7.58 (dd, J = 8.5 Hz; 5.0 Hz, 1H), δ 7.58 (dd, J = 8.0 Hz; 5.0 Hz, 1H), δ 8.18 (d, J = 8.5 Hz, 1H), δ 8.29
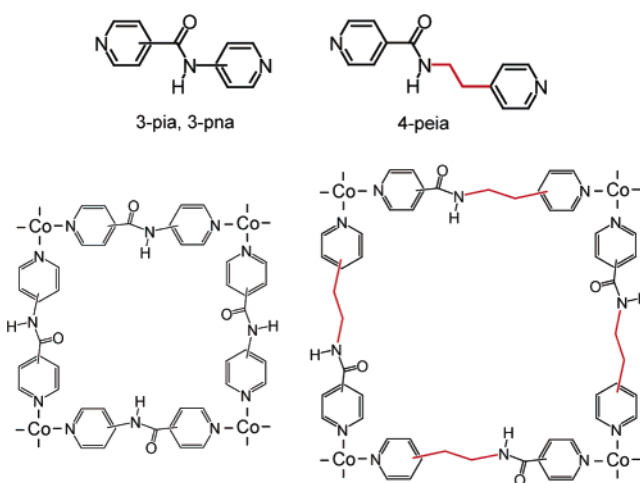
(d, J = 8.0 Hz, 1H), δ 8.33 (d, J = 5.0 Hz, 1H), δ 8.78 (d, J = 5.0 Hz, 1H), δ 8.92 (s, 1H), δ 9.12 (s, 1H), δ 10.64 (s, 1H). Elemental analysis calcd for C₁₁H₉N₃O (199.2): C, 66.32; H, 4.55; N, 21.09. Found: C, 65.80; H, 4.47; N, 20.89.

Synthesis of N-(2-Pyridin-4-yl-ethyl)-isonicotinamide (4-peia). The ligand was prepared by the reaction of isonicotinic chloride hydrochloride (15.0 g, 84.4 mmol) with 4-(2-aminoethyl)pyridine (10.0 mL, 84.4 mmol) in dry tetrahydrofuran (280 mL) in the presence of triethylamine (24 mL, 170 mmol) under N₂. The product was recrystallized from acetone/hexane in 55% yield (10.6 g). ¹H NMR (DMSO): δ 2.87 (t, J = 7.0 Hz, 2H), δ 3.54 (q, J = 7.0 Hz, 2H), δ 7.26 (d, J = 4.5 Hz, 2H), δ 7.67 (d, J = 4.5 Hz, 2H), δ 8.45 (d, J = 4.5 Hz, 2H), δ 8.70 (d, J = 4.5 Hz, 2H), δ 8.86 (t, J = 7.0 Hz, 1H). Elemental analysis calcd for C₁₃H₁₃N₃O (227.3): C, 68.70; H, 5.77; N, 18.49. Found: C, 68.56; H, 5.74; N, 18.54.

[Co(NO₃)₂(3-pna)₂]ₙ (1). An ethanol solution (1.5 mL) of 3-pna (29.9 mg, 1.5 mmol) was carefully layered on an acetone/chloroform mixed (v/v 9:1) solvent (1.5 mL) of Co(NO₃)₂ (21.8 mg, 0.75 mmol), where a mixed solvent of ethanol/chloroform (v/v 19:1) was placed between two layers (yield: 37%). Elemental analysis calcd for C₂₂H₁₈CoN₈O₈ (581.4): C, 45.45; H, 3.12; N, 19.27. Found: C, 44.80; H, 3.23; N, 19.06.

[CoBr₂(3-pna)₂]ₙ (2). An ethanol solution (1.5 mL) of 3-pna (14.9 mg, 0.075 mmol) was carefully layered on a methanol/chloroform mixed (v/v 9:1) solvent (1.5 mL) of CoBr₂ (8.2 mg, 0.038 mmol), where a mixed solvent of ethanol/chloroform (v/v 19:1) was placed between two layers (yield: 22%). Elemental analysis calcd for C₂₂H₁₈Br₂CoN₆O₂ (617.2): C, 42.81; H, 2.94; N, 13.62. Found: C, 42.31; H, 3.31; N, 12.92.

{[Co(NCS)₂(4-peia)₂]·4Me₂CO}ₙ (3 ⊃ 4Me₂CO). A solution of 4-peia (6.81 mg, 0.03 mmol) in acetone (1.5 mL) was gently layered onto a solution of Co(SCN)₂ (2.63 mg, 0.015 mmol) in acetone/chloroform (v/v 9:1, 1.5 mL), with a mixed solvent of acetone/chloroform (v/v 19:1, 1.5 mL) placed between the two layers (yield: 50%). For elemental analysis these crystals were collected and dried in vacuo at room temperature for 24 h. Elemental analysis calcd for C₃₁H₃₂CoN₈O₃S₂ (687.7): C, 54.14; H, 4.69; N, 16.29. Found: C, 53.47; H, 4.55; N, 16.10. The microcrystalline sample for physicochemical measurements was prepared in the same solvent, and the crystallinity was checked by X-ray powder diffraction as shown in Figure S1 in the Supporting Information.

X-ray Crystal Structure Determination. For each compound, a single crystal was mounted on a glass fiber and coated with epoxy resin. X-ray data collection for each crystal was carried out on a Rigaku Mercury diffractometer with graphite monochromated Mo Kα radiation (λ = 0.71069 Å) and a CCD 2-D detector. The size of the unit cells were calculated from the reflections collected on the setting angles of

(64) Bong, D. T.; Clark, T. D.; Granja, J. R.; Ghadiri, M. R. *Angew. Chem., Int. Ed.* **2001**, *40*, 988−1011.
(65) Ghadiri, M. R.; Granja, J. R.; Milligan, R. A.; McRee, D. E.; Khazanovich, N. *Nature* **1993**, *366*, 324−327.

Table 1. Crystal Data and Structure Refinement for [Co(NO$_3$)$_2$(3-pna)$_2$]$_n$ (**1**), [CoBr$_2$(3-pna)$_2$]$_n$ (**2**), and {[Co(NCS)$_2$(4-peia)$_2$]·4Me$_2$CO}$_n$ (**3** ⊃ **4Me$_2$CO**)

compound	1	2	3 ⊃ 4Me$_2$CO
chemical formula	C$_{22}$H$_{18}$CoN$_8$O$_8$	C$_{22}$H$_{16}$Br$_2$CoN$_6$O$_2$	C$_{40}$H$_{26}$CoN$_8$O$_6$S$_2$
formula weight	581.37	615.15	837.75
crystal dimensions (mm)	0.40 × 0.30 × 0.20	0.25 × 0.20 × 0.10	0.50 × 0.40 × 0.30
crystal system	orthorhombic	orthorhombic	monoclinic
space group	*Pbcn*	*Ccca*	*P*2$_1$/*c*
a (Å)	18.3004(6)	10.481(7)	11.115(3)
b (Å)	10.759(3)	19.03(1)	22.046(7)
c (Å)	11.458(2)	10.894(8)	9.717(3)
α (deg)	90	90	90
β (deg)	90	90	100.834(7)
γ (deg)	90	90	90
V (Å^3)	2255.9(8)	2172(2)	2338(1)
Z	4	4	2
ρ_{calcd} (g cm^{-3})	1.712	1.881	1.190
F(000)	1188	1212	858
μ (mm^{-1})	0.832	4.515	0.505
radiation (Å)	0.71069	0.71069	0.71069
temp (K)	223	293	293
2θ range	5.5° < 2θ < 54.1°	5.5° < 2θ < 54.9°	5.5° < 2θ < 55.0°
GOF	1.45	1.44	2.58
no. of data collected	11611	11978	24767
no. of unique data	1673	1211	5324
no. of obsd data	1673	1211	2526 (*I* > 5.00σ(*I*))
no. of variables	167	86	195
R[a]	0.066	0.053	0.083
R$_w$	0.125[b]	0.137[b]	0.132[c]

[a] $R = \Sigma||F_o| - |F_c||/\Sigma|F_o|$. [b] $R_w = \{\Sigma w[(F_o{}^2 - F_c{}^2)^2]/[(\Sigma wF_o{}^2)^2]\}^{1/2}$. [c] $R_w = [\Sigma w(|F_o| - |F_c|)^2/(\Sigma wF_o{}^2]^{1/2}$.

six frames by changing by 0.5° for each frame. Three different settings were used and were changed by 0.5° per frame. Intensity data were collected with a scan width of 0.5°. Empirical absorption correction by using REQABA[66] was performed for all data. For **1**, the structure was solved by direct methods by using the SIR88 program[67] and expanded by using Fourier techniques.[68] For **2**, the structure was solved by Patterson methods by using the DIRDIF94 program[69] and expanded by using Fourier techniques.[68] For **3** ⊃ **4Me$_2$CO**, the structure was solved by direct methods by using the SIR97 program[70] and expanded by using Fourier techniques.[68] All calculations were performed with the teXsan crystallographic software package from Molecular Structure Corporation.[71] For all compounds, the non-hydrogen atoms were refined anisotropically and all hydrogen atoms were placed in the ideal positions. In compound **1**, nitrate anions containing O(3) and 3-pna containing C(7) were refined isotropically. In compound **3** ⊃ **4Me$_2$CO**, acetone molecules containing O(2), O(3), and C(15)−C(20) were found at the final stage, and thus its atom positions were isotropically refined under a rigid condition.

Physical Measurements. Thermal gravimetry (TG) was carried out with a Rigaku Instrument TG8120 in a nitrogen atmosphere. IR spectra were recorded on a Perkin-Elmer 2000 FTIR spectrophotometer with samples prepared with Nujol. X-ray powder diffraction (XRPD) data were collected on a Rigaku RINT-2200HF (Ultima) diffractometer with Cu Kα radiation. Continuous-wave (CW) EPR spectra were recorded on a JEOL RE-3X spectrometer equipped with an Air-Product Heli-

Tran cryostat. The microwave frequency was measured using an Advantest R5372 frequency counter, and the magnetic field was repeatedly calibrated with diphenylpicrylhydrazyl (DPPH) and Mn^{2+} in MgO.

Measurement of Adsorption. The adsorption isotherm of CH$_4$ was measured by using FMS-BG gravimetric adsorption equipment from BEL Japan. The adsorption isotherms and kinetics measurements of gaseous acetone and N$_2$ were measured by using BELSORP18-Plus volumetric adsorption equipment from BEL Japan. In the sample chamber (∼17.5 mL) maintained at *T* ± 0.03 K was placed the adsorbent sample (∼50 mg), which had been prepared at 373 K and 10^{-1} Pa prior to measurement of the isotherms. The larger gas chamber (179.85 mL) with a pressure gauge was kept at (*T* + 20) ± 0.1 K. The acetone used to generate the vapor was degassed fully by repeated evacuation and vapor equilibration cycles of the liquid supply side of the vapor reservoir. Helium gas at a certain pressure was introduced in the gas chamber and was allowed to diffuse into the sample chamber by opening a valve. The change in pressure allowed an accurate determination of the volume of the total gas phase. The complexation was monitored in a similar manner by using a guest vapor in place of helium. The amount of guest adsorbed was calculated readily from pressure difference ($P_{cal} - P_e$), where P_{cal} is the calculated pressure with no guest adsorption and P_e is the observed equilibrium pressure. All operations were computer-controlled and automatic.

Results and Discussion

Crystal Structures. Crystallographic data for **1**−**3** are summarized in Table 1.

[Co(NO$_3$)$_2$(3-pna)$_2$]$_n$ (1). In **1**, the cobalt(II) center is octahedrally coordinated to each nitrogen atom of four 3-pna in equatorial plane, where two types of the nitrogen donors, carbonylpyridyl (N^C), and amino pyridyl (N^A), are located in a cis fashion (Figure 1a). The two Co−N bond distances are close to each other: Co−N(1) = 2.174(5) Å, Co−N(2) = 2.167(5) Å. In addition, the two oxygen atoms of NO$_3^-$ groups are coordinated axially with the distance of 2.089(5) Å. The cis N−Co−N or N−Co−O bond angles range from 83 to 104°,

(66) Jacobson, R. A. *REQABA Empirical Absorption Correction,* version 1.1-0301998; Molecular Structure Corp.: The Woodlands, TX, 1996−1998.
(67) Burla, M. C.; Camalli, M.; Cascarano, C.; Giacovazzo, C.; Polidori, G.; Spagna, R.; Viterbo, D. *J. Appl. Crystallogr.* **1989**, *22*, 389−303.
(68) Beurskens, P. T.; Admiraal, G.; Beurskens, G.; Bosman, W. P.; deGelder, R.; Israel, R.; Smits, J. M. M. *The DIRDIF-94 Program System*; Technical Report of the Crystallography Laboratory; University of Nijmegen: Nijmegen, The Netherlands, 1994.
(69) Beurskens, P. T.; Admiraal, G.; Beurskens, G.; Bosman, W. P.; Garcia-Granda, S.; Gould, R. O.; Smits, J. M. M.; Smykalla, C. *The DIRDIF Program System*; Technical Report of the Crystallography Laboratory; University of Nijmegen: Nijmegen, The Netherlands, 1992.
(70) Altomare, A.; Burla, M. C.; Camalli, M.; Cascarano, G. L.; Giacovazzo, C.; Guagliardi, A.; Moliterni, A. G. G.; Polidori, G.; Spagna, R. *J. Appl. Crystallogr.* **1999**, *32*, 115−119.
(71) *teXsan Crystal Structure Analysis Package*; Molecular structure Corporation: The Woodlands, TX, 2000.
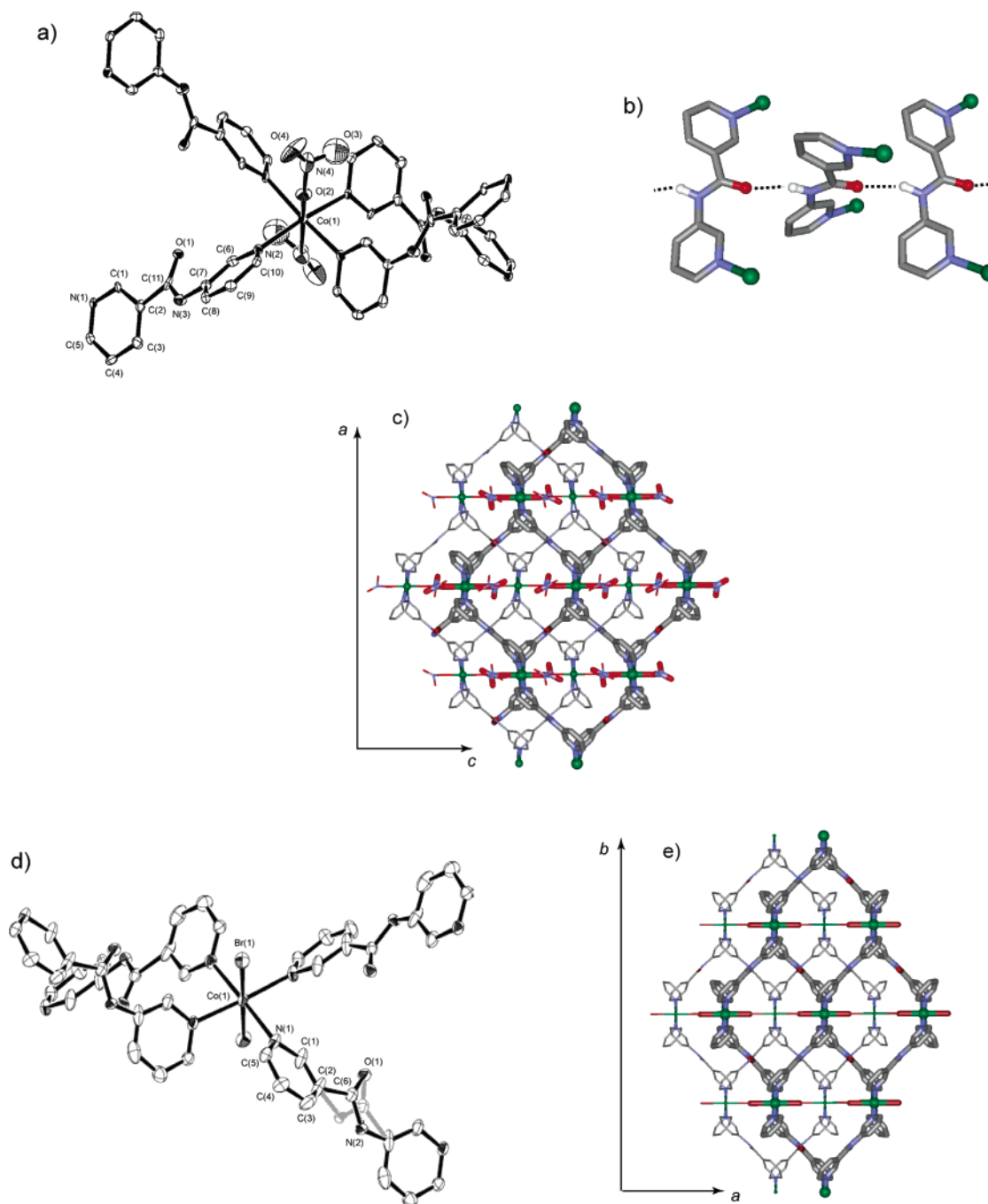
Figure 1. Crystal structure of [Co(NO$_3$)$_2$(3-pna)$_2$]$_n$ (**1**) and [Co(Br)$_2$(3-pna)$_2$]$_n$ (**2**). (a) ORTEP drawing of the cobalt center of **1** at the 30% probability level. Hydrogen atoms are omitted for clarity. (b) Crystal view of complementary hydrogen bonds among amide moieties in **1**. (c) Crystal view of **1** along the *b* axis. Two-layer stack with hydrogen bond of amide moieties between the layers. The thin and thick lines show the upper and lower layer, respectively. (d) ORTEP drawing of the cobalt center of **2** at the 30% probability level. Hydrogen atoms are omitted for clarity. The amide moiety is disordered about the 2-fold axis running through the 3-pna ligand. (e) Crystal view of **2** along the *c* axis. Two-layer stack with hydrogen bonds of amide moieties between the layers. The thin and thick lines show the upper and lower layer, respectively.

indicative of a distorted octahedral environment. The cobalt ions are linked by 3-pna to yield a honeycomb-shaped grid with the dimension of 10.8 Å × 10.8 Å. The square grids do not interpenetrate, affording a layered structure. It is worth noting that hydrogen-bonding links of the NH- - -O=C (N- - -O = 3.170(7) Å) groups between the adjacent layers create a complementary-amide binding network (Figure 1b). Adjacent layers are slipped in one direction by approximately 5.7 Å so that the axial NO$_3^-$ groups on one layer project into the channels along the *b* axis (Figure 1c). The framework contains no solvent

molecules, attributed to a closely packed layer structure with hydrogen bonds between the layers. The nearest Co–Co distance is about 10.8 Å in a layer and 7.5 Å in the adjacent layer.

[Co(Br)$_2$(3-pna)$_2$]$_n$ (2). In **2**, the cobalt(II) center is also coordinated to the four nitrogen atoms of 3-pna in equatorial plane (Figure 1d). In addition, two bromide atoms are coordinated axially with the distance of 2.594(2) Å. The trans Br–Co–Br bond angle is 180°. The cis N–Co–N bond angles range from 87 to 93°, indicative of a distorted octahedron. The cobalt ions are linked by 3-pna to afford a honeycomb-shaped grid
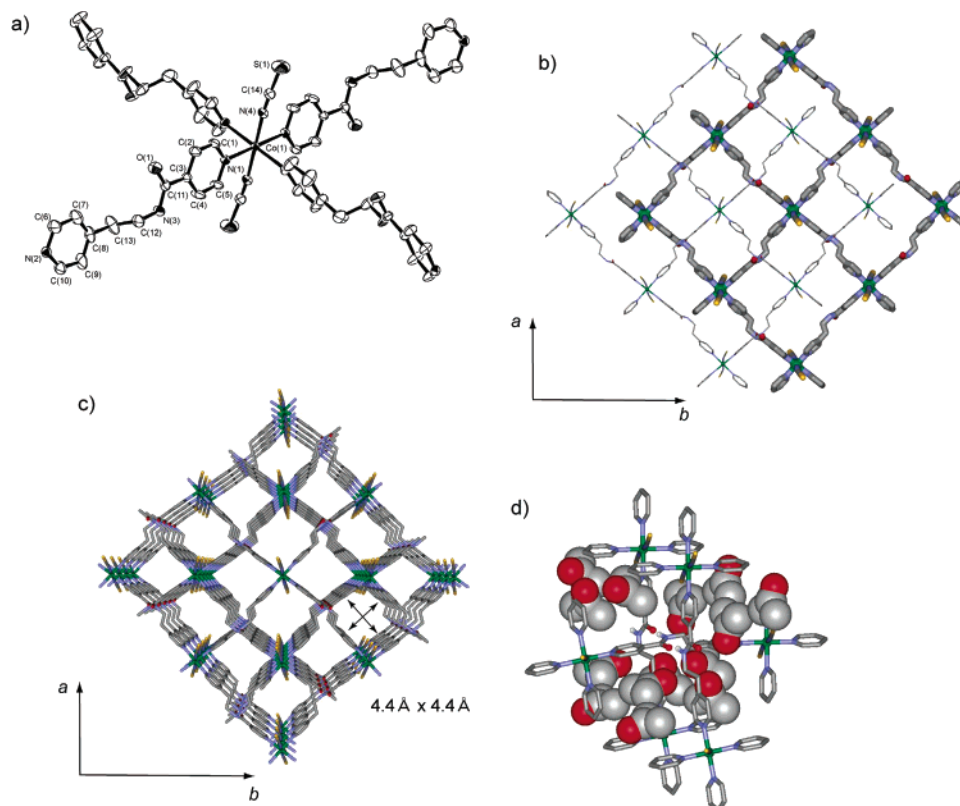
Figure 2. Crystal structure of {[Co(NCS)₂(4-peia)₂]·4Me₂CO}ₙ (3 ⊃ 4Me₂CO). (a) ORTEP drawing of the cobalt center of **3 ⊃ 4Me₂CO** at the 30% probability level. Hydrogen atoms and acetone molecules are omitted for clarity. (b) Two-layer stack of **3 ⊃ 4Me₂CO** along the *c* axis with hydrogen bonds of amide moieties between the layers. Acetone molecules are omitted for clarity. The thin and thick lines show the upper and lower layer, respectively. (c) Crystal structure of **3 ⊃ 4Me₂CO** along the *c* axis without acetone molecules. (d) Crystal view of **3 ⊃ 4Me₂CO** around complementary hydrogen bonds among amide moieties. Acetone molecules are represented by the space-filling model.

with the dimension of 10.9 Å × 10.9 Å (Figure 1e), as well as **1**. These layers also do not interpenetrate, affording a layered structure. As shown in Figure 1d, the amide moiety is disordered about the 2-fold axis running through the 3-pna ligands. Noticeably, the 2-D layers stack in a slipped fashion along the *a* axis with hydrogen bonding links of NH- - -O=C (N- - -O = 3.263(8) Å) between the layers. Coordinated bromide anions on one layer project into the channels along the *c* axis with a close distance of Br- - -Br = 5.294(4) Å. The nearest Co−Co distance is about 10.5 Å in a layer and 7.6 Å in the adjacent layer.

{[Co(NCS)₂(4-peia)₂]·4Me₂CO}ₙ (3 ⊃ 4Me₂CO). In **3 ⊃ 4Me₂CO**, the cobalt(II) center is octahedrally coordinated to each nitrogen atom of four 4-peia in equatorial plane, where two types of the nitrogen donors, carbonylpyridyl (N^C) and ethylpyridyl (N^E), are located in a trans fashion (Figure 2a). All the Co−N bond distances are close to each other: Co−N^C = 2.220(5) Å, Co−N^E = 2.191(6) Å. The trans N−Co−N bond angles for NCS and pyridine ligands are 180°. The cis N−Co−N bond angles range from 88.2(2) to 91.8(2)°. The NCS groups are coordinated axially in a slightly bending mode with the angles of 172.5(6)° (Co−N(4)−C(14)) and 177.3(8)° (N−C− S). The cobalt ions are linked by 4-peia to form a 2-D layer composed of a square grid motif with the dimension of 15.8 Å × 15.8 Å. Interestingly, the adjacent layers stack along the *c* axis with an offset by 0.5(*a* + *b*) along the *ab* plane, and the NCS group protrudes through the midpoint of the cavity of the adjacent layer eschewing interpenetration (Figure 2b). It is worth noting that hydrogen-bonding links of the NH- - -O=C (N- - -

O = 2.780(7) Å) groups between the adjacent layers create a complementary amide binding network. A channel with the dimension of 4.4 Å × 4.4 Å is observed[72] running along the *c* axis, despite the mutual slip of the neighboring layers (Figure 2b,c). These channels create a 46% void, where acetone molecules are accommodated with no significant interaction (Figure 2d). All pyridine planes in this crystal are parallel to the *c* axis, forming interior panels and, therefore, resulting in hydrophobic space. Acetone molecules show a guest column in the channel, but it is highly disordered. The ethylene moiety in 4-peia assumes a staggered ethane conformation about the C−C bond. The hydrogen bonds between the amide groups afford a dipole vector array; however, these dipole vectors are canceled out with the neighboring one. Compound **3 ⊃ 4THF**, which includes THF molecules, has similar cell parameters and isostructure as **3 ⊃ 4Me₂CO**. **3 ⊃ 4THF** also forms 2-D layers which are connected by a hydrogen-bonding link (NH- - -O= C (N- - -O = 2.79(1) Å) between the adjacent layers as shown in the Supporting Information.

Comparison of 1−3 with Other Square Grids. Selected 2-D square grids composed of octahedral metal cations and bpy (4,4′-bipyridine) analogues (=1:2) are summarized in Table 2. From Co(NCS)₂ and bpy analogues (=1:2), 2-D layers are rationally obtained because two thiocyanate ions tend to terminally coordinate to a cobalt(II) ion at the axial position.[19,48,49,56] What is important at this stage is the mutual relationship between the layer motifs. Among compounds

---

(72) The size is measured by considering van der Waals radii for constituting atoms. Hereafter, all the size estimation of pore is made in this way.

Table 2. Summary of the Bridging Ligands, Ligand Lengths, Open Areas, and Stacking Manners Found in Selected Square Grids

ligand	ligand length (Å)	open area (Å²)^c	stacking manner^d	metal + anion	reference
pyrazine	2.8	none	(iii)	Co(II) + SCN⁻	48
pyrazine	2.8	none	(iii)	Zn(II) + Br⁻	47
4,4′-bipyridine	7.1	none	(ii)	Zn(II) + SiF₆⁻	42
4,4′-bipyridine	7.1	6.8	(iii)	Cd(II) + NO₃⁻	12
4,4′-bipyridine	7.1	16.4	(iii)	Co(II) + SCN⁻	48
py-CH₂CH₂-py	9.4	none	(ii)	Co(II) + SCN⁻	56
py-CHCH-py	9.5	none	(ii)	Co(II) + SCN⁻	56
mppe^a	9.5	none	(ii)	Co(II) + SCN⁻	63
py-azo-py	9.0	9.0	(ii)	Co(II) + SCN⁻	49
py-antharacene-py	11.4	17.6	(i)	Ni(II) + NO₃⁻	46
py-Ph-py	11.4	4.2	(iii), HB^e	Ni(II) + NO₃⁻	46
py-PhPh-py	15.7	47.3	(iii), HB^e	Ni(II) + NO₃⁻	43
py-X-py^b	19.8	11.5	(iii)	Cu(II) + NO₃⁻	44
3-pia (guest = EtOH, H₂O)	8.5	9.0 × 2.5	(i)	Co(II) + SCN⁻	19
3-pia (guest = Me₂CO)	8.5	3.5 × 10.5	(i)	Co(II) + SCN⁻	19
3-pna	8.4	none	(iii), HB^e	Co(II) + SCN⁻	19
4-peia (**3 ⊃ 4Me₂CO**)	11.4	19.4	(iii), HB^e	Co(II) + SCN⁻	this study

^{a} 1-Methyl-1′-(4-pyridyl)-2-(4-pyrimidyl)ethylene. ^{b} 9,9-Bis[(S)-2-methylbutyl]-2,7-bis(4-pyridylethynyl)fluorine. ^{c} The size is measured by considering the van der Waals radii for constituent atoms. ^{d} Three types of packing manner are typically observed: (i) edge-to-edge manner, (ii) interpenetration, and (iii) staggered manner (see Scheme 2). ^{e} Each sheet is connected with an adjacent sheet by an interlayer hydrogen bond.

synthesized to date, a ligand longer than bpy prefers the formation of interpenetrating (type ii) to noninterpenetrating grid structures (see Scheme 2),[1] precluding their frames from porous materials. On the other hand, short bridging ligands favor the formation of the staggered fashion of grids in the adjacent layers (type iii), resulting in no pores. Therefore, to create useful cavities, a certain gadget is required. Inspection of Table 2 reveals that the gadgets are (1) template of guests[43,46] or (2) interlayer hydrogen bonds with a staggered fashion.[19,43,46]

To attain a pore frame, each grid must preclude interpenetration. Herein, "Coordination Polymer with Amide Groups" fulfills that requirement because complementary hydrogen bonds between amide moieties in neighboring layers take an important role in superposing each layers in staggered fashion. In **1** and **2**, despite the difference in counteranions, all square grids show staggered relationship ascribed to complementary amide binding. Although interpenetration is eschewed, "ABAB" stacking does not afford channels due to cavities occupied with metals and anions in neighboring layers. In **3 ⊃ 4Me₂CO** containing relatively longer 4-peia ligands, 1-dimensional (1-D) channels successfully form, because the SCN groups protrude perpendicular to layers. Moreover, 2-D layers of {[Co(NCS)₂(3-pia)₂]· 2EtOH·11H₂O}$_n$ and {[Co(NCS)₂(3-pia)₂]·4Me₂CO}$_n$ (3-pia = N-3-pyridylisonicotinamide) form in an edge-to-edge manner (type i) and afford channels, which accommodate guest molecules by hydrogen bonds with the amide group.[19] Therefore, "Coordination Polymer with Amide Groups" is suitable for construction of channels.

Thermal Analysis of 3 ⊃ 4Me₂CO. As seen in crystal structure analysis, **3 ⊃ 4Me₂CO** includes acetone molecules as a guest. The acetone desorption was monitored by TG. Figure 3 shows the TG thermograms for **3 ⊃ 4Me₂CO** over the temperature range from 30 to 500 °C at a heating rate of β = 5 °C/min. The observed weight loss of acetone molecules is in agreement with that calculated for the corresponding crystal structure. The TG data for compound **3 ⊃ 4Me₂CO** indicate two stages for weight loss of the guest molecules: three acetone molecules (observed 19.0%, calculated 20.2%) in the temperature range 30−80 °C, immediately followed by another weight loss of one acetone molecule (observed 4.3%, calculated 6.7%). The resultant species, [Co(NCS)₂(4-peia)₂]$_n$ (**3**), is stable up to
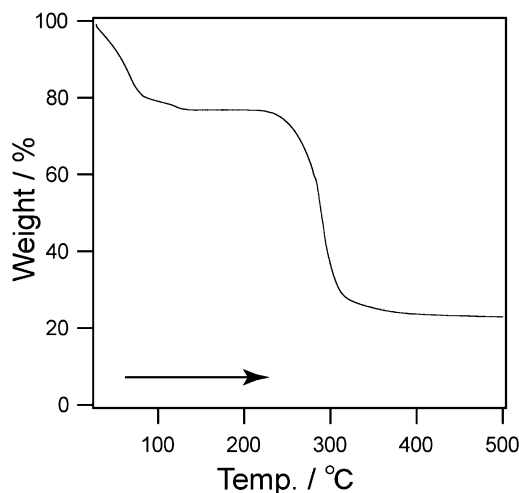

Figure 3. TG analysis of **3 ⊃ 4Me₂CO** over the temperature range from 30 to 500 °C at a heating rate of β = 5 °C/min under the N₂ atmosphere.

215 °C and then gradually decomposes with loss of two 4-peia ligands (observed 53.7%, calculated 52.7%).

Recoverable Collapsing of 3 ⊃ 4Me₂CO. Removal of the guest molecules causes a significant change on the framework of **3 ⊃ 4Me₂CO**. The two stages on desorption by heating **3 ⊃ 4Me₂CO** reveal the formation of [Co(NCS)₂(4-peia)₂]$_n$ (**3**) via {[Co(NCS)₂(4-peia)₂]·Me₂CO}$_n$ (**3 ⊃ Me₂CO**). **3 ⊃ Me₂CO** was also obtained by treating **3 ⊃ 4Me₂CO** under reduced pressure at room temperature, which was readily detected by XRPD and IR. The XRPD pattern of **3 ⊃ Me₂CO** shows an amorphous form with submaximum peaks (Figure 4b). Since positions of those submaximum peaks are different from those in **3 ⊃ 4Me₂CO**, **3 ⊃ Me₂CO** is a new form. Guest-free solid, **3**, was obtained by treating **3 ⊃ 4Me₂CO** under reduced pressure at 373 K. The framework of **3 ⊃ 4Me₂CO** cannot withstand a high level of stress on an extensive loss of the guest, resulting in an amorphous form as shown in Figure 4c. On the other hand, the XRPD pattern in Figure 4d is in good agreement with those of as-synthesized and calculated from single-crystal data of **3 ⊃ 4Me₂CO**. Therefore, it is concluded that the original crystal structure comes back completely upon being exposed to acetone vapor.
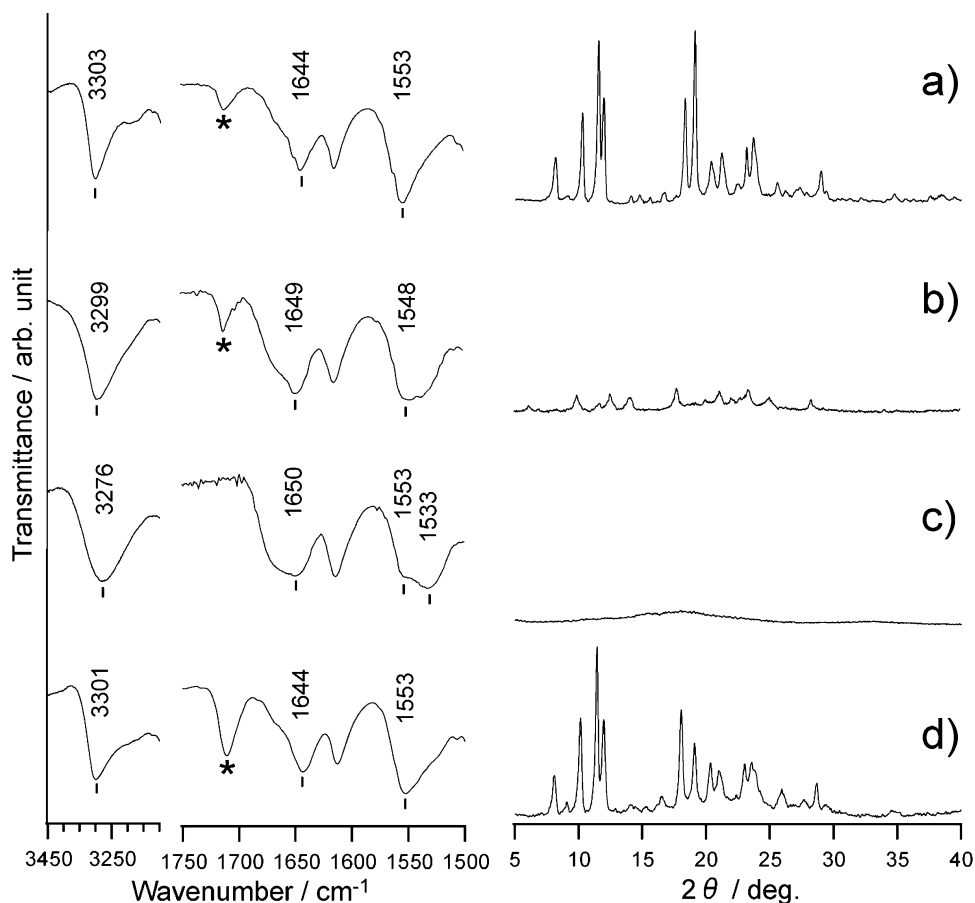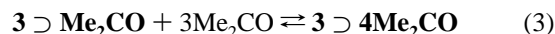
Figure 4. XRPD patterns (right) and IR spectra (left) in the region of N–H stretching, amide-I and amide-II bands at room temperature of (a) as-synthesized **3 ⊃ 4Me₂CO**, (b) **3 ⊃ Me₂CO** obtained by drying **3 ⊃ 4Me₂CO** in vacuo for 20 h at room temperature, (c) **3** obtained by drying **3 ⊃ 4Me₂CO** in vacuo for 20 h at 373 K, and (d) **3 ⊃ 4Me₂CO** obtained by exposing **3** to an acetone vapor for 4 days. Asterisk exhibits the C=O stretching band of acetone molecule.

IR spectra show the information of the amide environments of **3 ⊃ Me₂CO** and **3**. The N–H stretching and amide-I/-II bands appear in the regions of 3500–3100 cm⁻¹ and 1700–1500 cm⁻¹, respectively.[65,73-75] The amide moieties in **3 ⊃ 4Me₂CO** provide structured bands which are characteristic of *s*-trans complementary amide hydrogen bond as shown in Figure 4a; N–H stretching vibration and the amide-I/-II bands are observed at 3303, 1644, and 1553 cm⁻¹, respectively. In **3 ⊃ Me₂CO**, the broadening of the bandwidth is observed at 3299, 1649, and 1548 cm⁻¹, respectively. In **3**, N–H stretching and amide-I/-II bands are observed at 3276, 1650, and 1533 cm⁻¹ (1553 cm⁻¹, shoulder), respectively, and they encounter further broadening. Since the amide-II is a bending band, the lower shifts indicate weakening of the hydrogen bonds.[73,76] Therefore, the strength of complementary amide–amide hydrogen bonds in **3** becomes weaker in **3 ⊃ 4Me₂CO**.

IR data also show the reconstruction of the porous structure by the complementary amide hydrogen bond; broader bands of **3** in the N–H stretching and amide-I/-II bands change to the original ones (3301, 1644, and 1553 cm⁻¹). "Amorphous **3** →

crystalline **3 ⊃ 4THF**" regeneration is also induced by THF vapor, which is shown in the Supporting Information. We concluded that there are three different states, characterized by guest accommodation, namely, {[Co(NCS)₂(4-peia)₂]·4Me₂CO}ₙ (**3 ⊃ 4Me₂CO**), {[Co(NCS)₂(4-peia)₂]·Me₂CO}ₙ (**3 ⊃ Me₂CO**), and [Co(NCS)₂(4-peia)₂]ₙ (**3**), which are summarized as reaction eqs 2 and 3:

$$\mathbf{3} + \mathrm{Me_2CO} \rightleftarrows \mathbf{3} \supset \mathbf{Me_2CO} \qquad (2)$$

$$\mathbf{3} \supset \mathbf{Me_2CO} + 3\mathrm{Me_2CO} \rightleftarrows \mathbf{3} \supset \mathbf{4Me_2CO} \qquad (3)$$

In addition to the information of hydrogen bonding modes among layers, it is necessary to investigate the integrity of layers in amorphous **3**. To gain information concerning the coordination structures around the Co^{II} ion in **3**, EPR measurements were performed. Figure 5 shows the EPR spectra of **3 ⊃ 4Me₂CO**, **3 ⊃ Me₂CO**, and **3** measured at ∼15 K. The EPR spectrum of **3 ⊃ 4Me₂CO** indicates well-resolved features, and their EPR parameters have been determined by computer simulation as g'_1, g'_2, g'_3 = 5.7, 4.0, 2.8; A_1 = 8.0 mT;[77] the peak-to-peak line widths W_1, W_2, W_3 = 20, 40, 25 mT. On the other hand, **3 ⊃ Me₂CO** and **3** exhibit broad EPR spectra in accordance with the amorphous nature of these compounds. The *g* values are estimated as $g'_{center} \approx 4.0$ (**3 ⊃ Me₂CO**) and $g'_{center} \approx 3.9$ (**3**).

(73) Bellamy, L. J. *Advances in Infrared Group Frequencies*; Methuen: London, 1968.
(74) Haris, P. I.; Chapman, D. *Biopolymers* **1995**, *37*, 251–263.
(75) Hartgerink, J. D.; Granja, J. R.; Milligan, R. A.; Ghadiri, M. R. *J. Am. Chem. Soc.* **1996**, *118*, 43–50.
(76) As the NH bond becomes longer (hydrogen bond becomes stronger) and easier to stretch, the orbitals of the nitrogen atom take on more *p* character, which makes the bond more directional and harder to bend. Therefore, hydrogen shifts the amide-II band to higher frequencies.
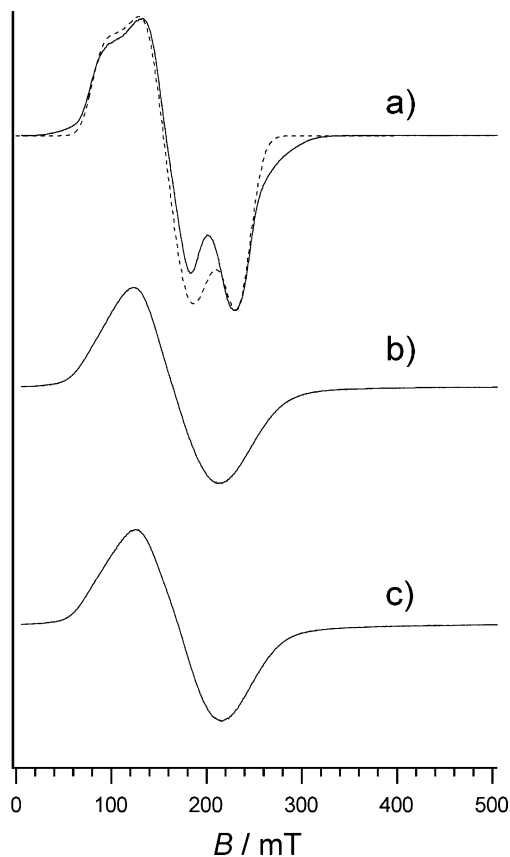
(77) Hyperfine coupling (HFC) is not included for the peaks g'_2, g'_3.

Figure 5. CW EPR spectra of powdered samples of (a) **3 ⊃ 4Me₂CO**, (b) **3 ⊃ Me₂CO**, and (c) **3**. Experimental setting: microwave frequency, (a) 8.998, (b) 8.993, and (c) 8.996 GHz. Microwave power, 1 mW; field modulation, 1 mT; temperature, 15 K.

(Computer simulation of the spectra of **3 ⊃ Me₂CO** and **3** was found to be difficult because of their broad nature.)

Several types of high-spin Co^{II} complexes have thus far been studied by EPR spectroscopy,[78] and the differences in the EPR pattern between tetrahedral and octahedral Co^{II} have been well-documented.[79−82] In tetrahedral Co^{II}, the ground orbital state is $^4A_2$, and thus the orbital angular momentum is well-quenched, which makes the spin Hamiltonian approach appropriate.[82,83] However, the observed g values for three compounds do not accord, similar to the case reported previously.[19] In the case of an octahedral Co^{II}, on the other hand, the ground orbital state is $^4T_1$, and thus orbital degeneracy still remains.[84] Theoretical treatment of the EPR parameters of octahedral Co^{II} was made by Abragam and Pryce,[85] who gave theoretical expressions for the effective g value and HFC parameters considering up to the second-order perturbation effects. The perturbation result for the effective g values are plotted against $\Delta/|\lambda|$, where Δ is
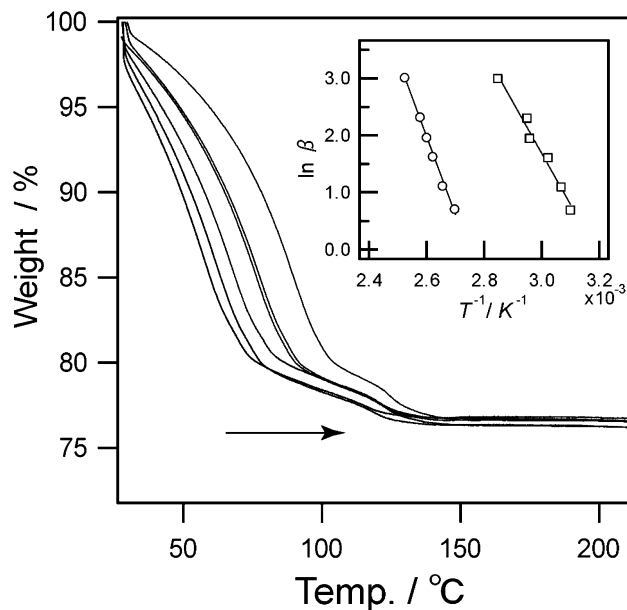
(78) Weckhuysen, B. M.; Verberckmoes, A. A.; Uytterhoeven, M. G.; Mabbs, F. E.; Collison, D.; Boer, E. d.; Schoonheydt, R. A. *J. Phys. Chem. B* **2000**, *104*, 37−42.
(79) Bencini, A.; Benelli, C.; Gattenschi, D.; Zanchini, C. *Inorg. Chem.* **1980**, *19*, 1301−1304.
(80) Banci, L.; Benelli, C.; Gatteschi, D.; Mani, F. *Inorg. Chem.* **1982**, *21*, 1133−1136.
(81) Makinen, M. W.; Kuo, L. C.; Yim, M. B.; Wells, G. B.; Fukuyama, J. M.; Kim, J. E. *J. Am. Chem. Soc.* **1985**, *107*, 5245−5255.
(82) Drulis, H.; Dyrek, K.; Hoffmann, K. P.; Hoffmann, S. K.; Weselucha-Birczynska, A. *Inorg. Chem.* **1985**, *24*, 4009−40125.
(83) Pilbrow, J. R. *J. Magn. Reson.* **1978**, *31*, 479−490.
(84) Griffith, J. S. In *The Theory of Transition Metal Ions*; Cambridge University Press: London, 1961.
(85) Abragam, A.; Pryce, M. H. *Proc. R. Soc. London, Ser. A* **1951**, *205*, 173−191.

Figure 6. Thermogravimetric curves of **3 ⊃ 4Me₂CO** plotted against the reciprocal absolute temperature. Heating rate: 2, 3, 5, 7, 10, and 20 °C/min. Insert: Plots of logarithms of heating rate (β) versus the conversions of reciprocal absolute temperature of 50% desorption for **3 ⊃ 4Me₂CO** (open squares) and **3 ⊃ Me₂CO** (open circles).

the ligand-field splitting between $|^4T_1;xy>$ and $|^4T_1;z>$ with the value being positive when $|^4T_1;z>$ is upper, and λ is the spin−orbit coupling constant. We estimate $\Delta/|\lambda| = 2.1$, ~ 0, ~ 0 for **3 ⊃ 4Me₂CO**, **3 ⊃ Me₂CO**, and **3**, respectively.[86] The present EPR results are in good agreement with the theory, and therefore, the Co^{II} ion in **3 ⊃ Me₂CO** and **3** are in octahedral coordination environment as well as **3 ⊃ 4Me₂CO**.

Throughout the characterization of series of **3** by XRPD, IR, and EPR, we conclude that the 2-D motif of **3** does not collapse. Although the layer framework in **3** is maintained, the XRPD pattern shows that **3** crystalline order over a long range is not seen (Figure 4c). The pattern is attributed to the random layer slip against the neighboring layers, accompanying with the deformation of grid framework.

Desorption and Energetics. As mentioned previously, **3 ⊃ 4Me₂CO** is desolvated, via **3 ⊃ Me₂CO**, to be amorphous **3**. In both desorption processes, "**3 ⊃ Me₂CO → 3**" and "**3 ⊃ 4Me₂CO → 3 ⊃ Me₂CO**", the activation energies of desorption (E_{de1} and E_{de2}, respectively) are estimated by recording TG curves at various heating rates (β) and by plotting $\log\beta$ vs $1/T$ at a given extent of desorption, according to the eq 4.[87,88]

$$\ln\beta = -1.0516E_{de}/RT + \text{constant} \qquad (4)$$

The results of the thermogravimetry at various heating rates are plotted against the reciprocal absolute temperature in Figure 6. It is apparent that these curves can be superposed by lateral shifts. For the process of "**3 ⊃ 4Me₂CO → 3 ⊃ Me₂CO**" at 50% desorption, $T = 49.6$ (322.6), 53.0 (326.0), 57.9 (330.9), 65.1 (338.1), 66.2 (339.2), and 78.3 °C (351.3 K) at $\beta = 2$, 3, 5, 7, 10, and 20 °C/min. For the process of "**3 ⊃ Me₂CO → 3**" at 50% desorption, $T = 97.4$ (370.4), 103.2 (376.2), 108.1

(86) Effective g values calculated from the first-order perturbation equations are plotted versus $\Delta/|\lambda|$ and are depicted in Figure S4.
(87) Flynn, J. H.; Wall, L. A. *J. Polym. Sci., Part B: Polym. Phys.* **1966**, *4*, 323−328.
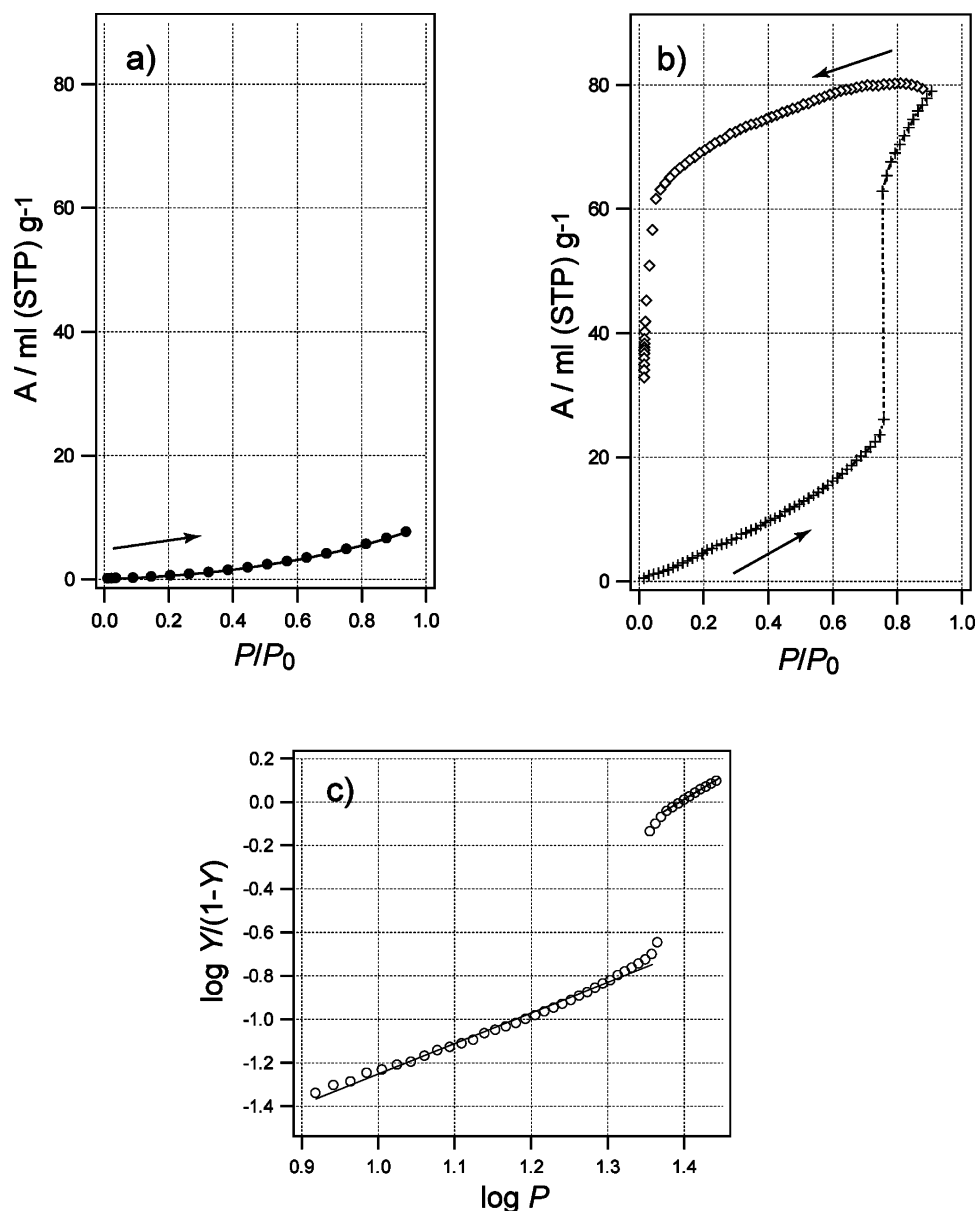(88) Ozawa, T. *Bull. Chem. Soc. Jpn.* **1965**, *38*, 1881−1886.

Figure 7. (a) Isotherm for N_2 adsorption (filled circles) at 77 K of **3** over the pressure range from 0.003 to 0.939 atoms. P_0 is a saturated vapor pressure, 1.022 atoms, of N_2 at 77 K. (b) Isotherm for acetone vapor adsorption (crosses) and desorption (open squares) at 298 K of **3** over the pressure range from 0.507 to 27.756 kPa. P_0 is a saturated vapor pressure, 30.593 kPa, of acetone at 298 K. (c) Hill plot for the adsorption curve of (b), where Y ($0 < Y < 1$) and P are the extent of complexation and pressure (kPa), respectively.

(381.1), 111.1 (384.1), 114.6 (387.6), and 122.8 °C (395.8 K) at β = 2, 3, 5, 7, 10, and 20 °C/min. In the insert of Figure 6, the logarithms of the heating rates are plotted against the reciprocal absolute temperature, until which point the weight of the sample decreases to a 50% desorption. Straight lines are obtained, and the method of the least squares affords the activation energies determined: E_{de1} = 108 kJ/mol and E_{de2} = 71 kJ/mol.

Isothermal Adsorption and Desorption Experiment. Recently, several articles on adsorption behavior of porous coordination polymers have been published.[2,14,19,20,27,89−93] When

one looks more carefully at the behavior of the adsorption, the actual porous coordination polymers, responsible for uptaking the adsorbates, tend to undergo guest-directed framework transformation,[19,20,27,92,94] dissimilar to zeolites and activated carbons. The mechanism of this transformation should be investigated in detail, and the present **3** system is suitable for in-depth study on adsorption and desorption properties.

3 shows no N_2 adsorption at 77 K as shown in Figure 7a. Moreover, the adsorption isotherm of CH_4 for **3** at 298 K reveals no uptake into the micropores but only surface adsorption.[95] These results indicate that **3** does not maintain channels available for N_2 (3.64 Å) and CH_4 molecules (3.8 Å).[20,93]

(89) Kondo, M.; Okubo, T.; Asami, A.; Noro, S.-I.; Yoshitomi, T.; Kitagawa, S.; Ishii, T.; Matsuzaka, H.; Seki, K. *Angew. Chem., Int. Ed.* **1999**, *38*, 140−143.
(90) Kepert, C. J.; Rosseinsky, M. J. *Chem. Commun.* **1999**, 375−376.
(91) Fletcher, A. J.; Cussen, E. J.; Prior, T. J.; Rosseinsky, M. J.; Kepert, C. J.; Thomas, K. M. *J. Am. Chem. Soc.* **2001**, *123*, 10001−10011.
(92) Li, D.; Kaneko, K. *Chem. Phys. Lett.* **2001**, *335*, 50−56.

(93) Pan, L.; Adams, K. M.; Hernandez, H. E.; Wang, X.; Zheng, C.; Hattori, Y.; Kaneko, K. *J. Am. Chem. Soc.* **2003**, *125*, 3062−3067.
(94) Dewa, T.; Endo, K.; Aoyama, Y. *J. Am. Chem. Soc.* **1998**, *120*, 8933−8940.
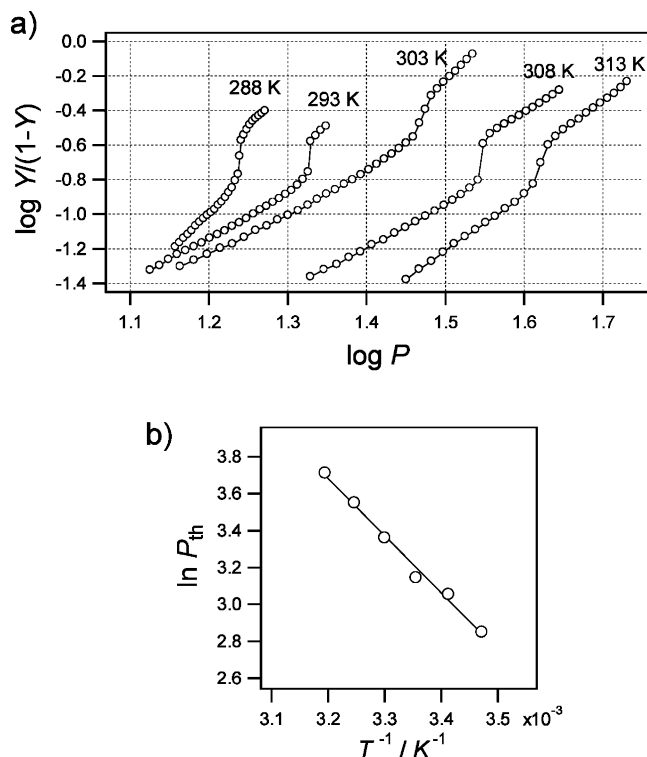(95) Isotherm for methane adsorption at 298 K of **3** from 0.5 to 70 atoms is depicted in Figure S5.

a)

b)

Figure 8. (a) Hill plot for the acetone adsorption curve of **3** at 288, 293, 303, 308, and 313 K. (b) Plot of ln P_{th} against T^{-1}.

Since **3** shows structural regeneration when exposed to acetone vapor, the acetone adsorption and desorption experiment was carried out on **3**. Figure 7b shows the adsorption and desorption isotherms for acetone over the relative pressure range from 0 to 0.9 at 298 K. The adsorption isotherm shows a slight increase and an abrupt rise at $P/P_0 = 0.76$. This characteristic adsorption profile clearly indicates a conversion of amorphous **3** to a crystalline **3** $\supset$ **4Me₂CO**.[92] On the other hand, the desorption isotherm shows a monotonic decrease as if the pores were maintained until a sudden drop at $P/P_0 = 0.05$. A large range of hysteresis loop based on the structural conversion is realized in this compound, which could not be obtained in rigid porous materials.

Threshold Points for Adsorption. Figure 7c shows the Hill plot (eq 5) of acetone adsorption on **3** at 298 K.

$$\log [Y/(1 - Y)] = n \log P + \log K \qquad (5)$$

where Y ($0 < Y < 1$) is the extent of complexation (adsorption), which is often used to describe cooperative or allosteric binding processes in homogeneous solutions. It may be more important, however, that this treatment of the binding data according to a homogeneous host−guest complexation fails to give a linear correlation for the whole pressure range. The acetone adsorption curve is characterized by a sharp threshold point (P_{th}) consisting of three stages, which are characterized by different slopes: a prebinding region at $P < P_{th}$, the vertical region at $P \cong P_{th}$, and a milder follow-up region at $P > P_{th}$. The vertical one at $P \cong P_{th}$ ($P_{th}/P_0 = 0.76$) indicates a remarkably cooperative nature of adsorption around P_{th}.

Isothermal acetone adsorption curves were obtained at various temperatures: 288, 293, 298, 303, 308, and 313 K. The three stages of the Hill plots are also observed for all the temperatures. Figure 8a clearly shows the dependence of P_{th} on the temper-

ature: the P_{th} values decrease with decrease in temperature: 17.3 (288), 21.2 (293), 23.2 (298), 28.8 (303), 34.8 (308) and 40.9 kPa (313 K). Since P_{th} values could be regarded as the equilibrium pressure for the reaction of acetone inclusion, their temperature dependence allows us to evaluate the associated enthalpy change on acetone adsorption process based on eq 6:

$$d \ln P_{th}/d(1/T) = \Delta H_{ad}/R \qquad (6)$$

where R and ΔH_{ad} denote the gas constant and the adsorption enthalpy of gas, respectively. The plot of ln P_{th} vs $1/T$, according to eq 6, yields a straight line (Figure 8b), whose slope leads to $\Delta H_{ad} = -25$ kJ/mol for the inclusion of acetone.

Mechanism and Thermodynamics in Relation to Structural Regeneration. **3** does not contain channels, but nevertheless undergoes the inclusion of acetone molecules. Several organic hosts and metal-organic architectures exhibit the ability to switch between dense and open forms responding to guest molecules.[94,96−105] The new aspect of **3** $\supset$ **4Me₂CO** is solid form conversion based on infinite 2-D layers bound by complementary hydrogen bonds. As mentioned previously, it is apparent that the 2-D structural integrity is maintained during the reaction. The structural regeneration by the inclusion of acetone is associated with change of the hydrogen-bonding mode: the accommodation of acetone molecules in each grid of the 2-D motif could control the orientation of the amide hydrogen bonds; thus, the overall relationship between the motifs comes back to the former **3** $\supset$ **4Me₂CO**, where extensive cooperativity must exist.

Previously, the energy diagram for the adsorption and desorption of some organic networks was fortunately constructed and reported.[94] In general, it is difficult to discuss the mechanism of a solid-state reaction, because the reaction is composed of many kinds of elementary reactions. Figure 9 shows a schematic energy diagram for the acetone adsorption and desorption of **3**, based on the results of TG and adsorption measurements. DSC measurement shows two separated endotherms of desorption for **3** $\supset$ **4Me₂CO**; however, it is difficult to estimate the desorption enthalpy because **3** $\supset$ **4Me₂CO** is unstable at room temperature and decomposes with loss of acetone molecules, usually with concomitant rearrangement of the host compound to the nonporous compound. Therefore, the energy difference among states could be calculated from ΔH_{ad} (-25 kJ/mol), that is, $\Delta H_{ad1} = \Delta H_{ad} = -25$ kJ/mol and $\Delta H_{ad2} = 3\Delta H_{ad} = -75$ kJ/mol, and activation energy ($E_{de1} = 108$ kJ/mol and $E_{de2} = 71$ kJ/mol) was obtained as mentioned previously. Although the thermal decomposition of **3** $\supset$ **4Me₂CO** → **3** $\supset$ **Me₂CO** is

(96) Miyata, M.; Shibakami, M.; Chirachanchai, S.; Takemoto, K.; Kasai, N.; Miki, K. *Nature* **1990**, *343*, 446−447.
(97) Bourne, S. A.; Nassimbeni, L. R.; Toda, F. *J. Chem. Soc., Perkin Trans. 2* **1991**, 1335−1341.
(98) Barbour, L. J.; Caira, M. R.; Coetzee, A.; Nassimbeni, L. R. *J. Chem. Soc., Perkin Trans. 2* **1995**, 1345−1349.
(99) Ung, A. T.; Gizachew, D.; Bishop, R.; Scudder, M. L.; Dance, I. G.; Craig, D. C. *J. Am. Chem. Soc.* **1995**, *117*, 8745−8756.
(100) Endo, K.; Sawaki, T.; Koyanagi, M.; Kobayashi, K.; Masuda, H.; Aoyama, Y. *J. Am. Chem. Soc.* **1995**, *117*, 8341−8352.
(101) Endo, K.; Koike, T.; Sawaki, T.; Hayashida, O.; Masuda, H.; Aoyama, Y. *J. Am. Chem. Soc.* **1997**, *119*, 4117−4122.
(102) Thaimattam, R.; Xue, F.; Sarma, J. A. R. P.; Mak, T. C. W.; Desiraju, G. R. *J. Am. Chem. Soc.* **2001**, *123*, 4432−4445.
(103) Atwood, J. L.; Barbour, L. J.; Jerga, A.; Schottel, B. L. *Science* **2002**, *298*, 1000−1002.
(104) Soldatov, D. V.; Ripmeester, J. A.; Shergina, S. I.; Sokolov, I. E.; Zanina, A. S.; Gromilov, S. A.; Dyadin, Y. A. *J. Am. Chem. Soc.* **1999**, *121*, 4179−4188.
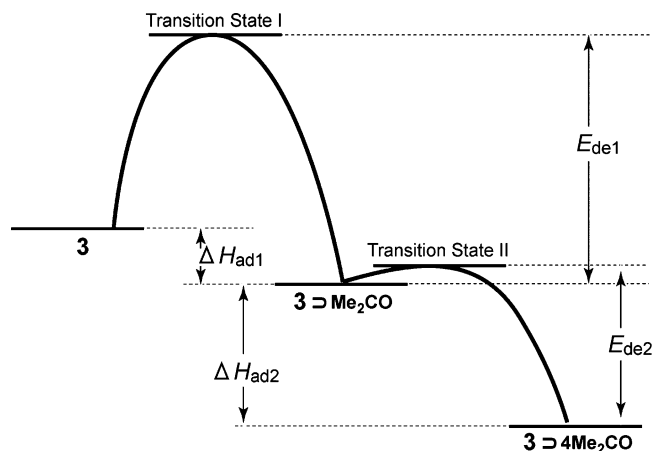(105) Soldatov, D. V.; Ripmeester, J. A. *Chem.−Eur. J.* **2001**, *7*, 2979−2994.

Figure 9. Schematic energy diagram for the solid−gas complexation of **3** with gaseous acetone. Definitions are as follows: E_{de1} and E_{de2} are activation energies of acetone desorption in the processes of $3 \supset Me_2CO \rightarrow 3$ and $3 \supset 4Me_2CO \rightarrow 3 \supset Me_2CO$, respectively. ΔH_{ad1} and ΔH_{ad2} are heats of guest binding in the processes of $3 \rightarrow 3 \supset Me_2CO$ and $3 \supset Me_2CO \rightarrow 3 \supset 4Me_2CO$, respectively.

an endothermic reaction, the activation energy ($E_{de2} = 71$ kJ/mol) is lower than the thermodynamic value for the reaction ($\Delta H_{ad2} = -75$ kJ/mol). This is because the activation energy is obtained based on the rate-determining step of some elementary reaction.

As seen in the energy diagram of the acetone adsorption process, **3** transfers to $3 \supset Me_2CO$ with the energy barrier and smoothly follows the second transformation to be $3 \supset 4Me_2CO$. It is surprising that acetone inclusion enthalpy (ΔH_{ad} (-25 kJ/mol)) is close to acetone vaporization enthalpy ($\Delta H_{vap} = 30.99$ kJ/mol).[106] Thus, even weak dispersive forces can exert a profound influence over solid-sate transformation.

Conclusion

This work demonstrates (1) the rational construction of flexible porous frameworks using square grids and (2) characterization of cooperative adsorption with thermal analysis. In addition, we showed a new contrivance for dynamic porous coordination polymers based on flexible amide−amide hydrogen bonds.

(106) Weast, R. C.; Astle, M. J.; Beyer, W. H. *CRC Handbook of Chemistry and Physics*, 80th ed.; CRC Press: Boca Raton, FL, 1999.

(1) From Co(SCN)$_2$ and bipyridyl derivatives containing an amide group, we succeeded in producing new square grid frameworks, **1**−**3**, which have complementary amide binding manner eschewing interpenetrating. Particularly, $3 \supset 4Me_2CO$ affords micropores fulfilled with guest molecules and shows that structural transformation via amorphous is caused by adsorption and desorption of guest molecules. Such flexible porous coordination polymers offer an application to a unique class of materials, which cannot be obtained in rigid porous material, in this case, large hysteresis loop on adsorption and desorption measurements, and leading to amplification of adsorption for specific guest.

(2) On the basis of well-defined $3 \supset 4Me_2CO$, the energy diagram was achieved. Our results imply that the coordination polymer is often much more dynamic than generally believed and that weak dispersive forces induce structural rearrangement in a well-concerted fashion. Although many porous coordination polymers have been synthesized and reported, to the best of our knowledge, the report of thermal analysis is sparse. Thermodynamic parameters calculated in the present course of study are also useful to analyze the thermal behavior of porous coordination polymers.

This research is particularly relevant in the context of solid-state chemistry since rational design of solids has important ramifications for the development of new materials with unusual properties. We anticipate this approach to be viable for the construction of cavity-containing frameworks possessing bridging ligands not described here, and we also anticipate this approach to be applicable for the design of flexible porous materials.

Supporting Information Available: XRPD, detailed crystal views, IR spectra of the materials (4-peia and Co(SCN)$_2$), effective *g* values of **3** plotted versus $\Delta/|\lambda|$, isotherm for CH$_4$ adsorption at 298 K of **3** (PDF), and X-ray crystallographic files (CIF) for **1**−**3**. This material is available free of charge via the Internet at http://pubs.acs.org.

JA039914M